

University of Wollongong

Research Online

---

Faculty of Engineering and Information  
Sciences - Papers: Part B

Faculty of Engineering and Information  
Sciences

---

2020

## A new AI-surrogate model for dynamics analysis of a magnetorheological damper in the semi-active seat suspension

Xinhua Liu

Ningning Wang

Kun Wang

Shumei Chen

Shuaishuai Sun

University of Wollongong, [ssun@uow.edu.au](mailto:ssun@uow.edu.au)

*See next page for additional authors*

Follow this and additional works at: <https://ro.uow.edu.au/eispapers1>



Part of the [Engineering Commons](#), and the [Science and Technology Studies Commons](#)

---

### Recommended Citation

Liu, Xinhua; Wang, Ningning; Wang, Kun; Chen, Shumei; Sun, Shuaishuai; Li, Zhixiong; and Li, Weihua, "A new AI-surrogate model for dynamics analysis of a magnetorheological damper in the semi-active seat suspension" (2020). *Faculty of Engineering and Information Sciences - Papers: Part B*. 3901. <https://ro.uow.edu.au/eispapers1/3901>

Research Online is the open access institutional repository for the University of Wollongong. For further information contact the UOW Library: [research-pubs@uow.edu.au](mailto:research-pubs@uow.edu.au)

---

# A new AI-surrogate model for dynamics analysis of a magnetorheological damper in the semi-active seat suspension

## Abstract

© 2020 The Author(s). Published by IOP Publishing Ltd. This paper aims to develop a surrogate model for dynamics analysis of a magnetorheological damper (MRD) in the semi-active seat suspension system. An improved fruit fly optimization algorithm (IFOA) which enhances the global search capability of the original FOA is proposed to optimize the structure of a back propagation neural network (BPNN) in establishing the surrogate model. An MRD platform was fabricated to generate experimental data to feed the IFOA-BPNN model. Intrinsic patterns about the MRD dynamics behind the datasets have been discovered to establish a reliable MRD surrogate model. The outputs of the surrogate model demonstrate satisfactory dynamics characteristics in consistence with the experimental results. Moreover, the performance of the IFOA-BPNN based surrogate model was compared with that produced by the BPNN based, genetic algorithm-BPNN based, and FOA-BPNN based surrogate models. The comparison result shows better tracking capacity of the proposed method on the hysteresis behaviors of the MRD. As a result, the newly developed surrogate model can be used as the basis for advanced controller design of the semi-active seat suspension system.

## Disciplines

Engineering | Science and Technology Studies

## Publication Details

Liu, X., Wang, N., Wang, K., Chen, S., Sun, S., Li, Z. & Li, W. (2020). A new AI-surrogate model for dynamics analysis of a magnetorheological damper in the semi-active seat suspension. *Smart Materials and Structures*, 29 (3),

## Authors

Xinhua Liu, Ningning Wang, Kun Wang, Shumei Chen, Shuaishuai Sun, Zhixiong Li, and Weihua Li

TECHNICAL NOTE • OPEN ACCESS

## A new AI-surrogate model for dynamics analysis of a magnetorheological damper in the semi-active seat suspension

To cite this article: Xinhua Liu *et al* 2020 *Smart Mater. Struct.* **29** 037001

View the [article online](#) for updates and enhancements.

## Technical Note

# A new AI-surrogate model for dynamics analysis of a magnetorheological damper in the semi-active seat suspension

Xinhua Liu<sup>1</sup>, Ningning Wang<sup>1</sup>, Kun Wang<sup>1</sup>, Shumei Chen<sup>2</sup>,  
Shuaishuai Sun<sup>3</sup>, Zhixiong Li<sup>4,5,6</sup> and Weihua Li<sup>4</sup>

<sup>1</sup> School of Mechanical and Electrical Engineering, China University of Mining & Technology, Xuzhou 221116, People's Republic of China

<sup>2</sup> Key Laboratory of Fluid Power and Intelligent Electro-Hydraulic Control (Fuzhou University), Fujian Province University, Fuzhou 350112, People's Republic of China

<sup>3</sup> New Industry Creation Hatchery Center, Tohoku University, Sendai 980-8577, Japan

<sup>4</sup> School of Mechanical, Materials, Mechatronic and Biomedical Engineering, University of Wollongong, Wollongong, NSW 2522, Australia

<sup>5</sup> Department of Marine Engineering, Ocean University of China, Tsingtao 266100, People's Republic of China

E-mail: [liuxinhua@cumt.edu.cn](mailto:liuxinhua@cumt.edu.cn), [wangning@cumt.edu.cn](mailto:wangning@cumt.edu.cn), [wangkuncumt@163.com](mailto:wangkuncumt@163.com), [smchen@fzu.edu.cn](mailto:smchen@fzu.edu.cn), [shuaishuai.sun.b1@tohoku.ac.jp](mailto:shuaishuai.sun.b1@tohoku.ac.jp), [zhixiong\\_li@uow.edu.au](mailto:zhixiong_li@uow.edu.au) and [weihuali@uow.edu.au](mailto:weihuali@uow.edu.au)

Received 13 August 2019, revised 10 December 2019

Accepted for publication 14 January 2020

Published 4 February 2020



CrossMark

## Abstract


This paper aims to develop a surrogate model for dynamics analysis of a magnetorheological damper (MRD) in the semi-active seat suspension system. An improved fruit fly optimization algorithm (IFOA) which enhances the global search capability of the original FOA is proposed to optimize the structure of a back propagation neural network (BPNN) in establishing the surrogate model. An MRD platform was fabricated to generate experimental data to feed the IFOA-BPNN model. Intrinsic patterns about the MRD dynamics behind the datasets have been discovered to establish a reliable MRD surrogate model. The outputs of the surrogate model demonstrate satisfactory dynamics characteristics in consistence with the experimental results. Moreover, the performance of the IFOA-BPNN based surrogate model was compared with that produced by the BPNN based, genetic algorithm-BPNN based, and FOA-BPNN based surrogate models. The comparison result shows better tracking capacity of the proposed method on the hysteresis behaviors of the MRD. As a result, the newly developed surrogate model can be used as the basis for advanced controller design of the semi-active seat suspension system.

Supplementary material for this article is available [online](#)

Keywords: magnetorheological damper, surrogate model, artificial intelligence

(Some figures may appear in colour only in the online journal)

<sup>6</sup> Author to whom any correspondence should be addressed.

 Original content from this work may be used under the terms of the [Creative Commons Attribution 3.0 licence](#). Any further distribution of this work must maintain attribution to the author(s) and the title of the work, journal citation and DOI.

## 1. Introduction

Human beings suffer an adverse reaction because of the high vibration intensity in a vehicle [1]. A seat suspension with excellent comfort and stability is an effective tool to solve the

hostile vibration problem. Compared to other existing seat suspension systems, semi-active seat suspension based on magnetorheological damper (MRD) has the advantages of simple structure, low power consumption and fast response. More importantly, the natural frequencies and damping characteristics of the semi-active seat suspension can be adjusted according to the external excitations [2–4]. As a result, by a suitable control strategy the MRD-suspension system can reduce the vibration level of the vehicles and provide smooth riders for passengers.

An accurate dynamic model of the MRD is essential to achieve the desirable vibration control for the suspension system. However, it is always a challenging task to establish an accurate MRD dynamic model due to strong nonlinear hysteresis [5]. Recent researches show the capability of artificial intelligence (AI)-based techniques in modeling the MRD dynamics by performing machine learning and data mining [6, 7]. In [8], a new algorithm named establishing neuro-fuzzy system was proposed to identify the dynamic characteristics of smart dampers, and the effectiveness of the proposed algorithm was verified. In [9], an adaptive neuro-fuzzy inference system was used to establish dynamic models for non-parametric smart dampers, and the superiority of the modeling method was demonstrated. Prior professional information and exact MRD parameters are not required in establishing the AI-based surrogate model. Among existing popular AI techniques back propagation neural network (BPNN) [10–13] has been widely used in information classification, pattern recognition, dynamic modeling and system prediction because of its simple structure, strong feasibility and parallel computing ability. However, the local optimum issue in the BPNN training process often affects the network performance and the steepest decent method reduces the learning efficiency [14, 15]. In order to solve this problem, intelligent optimization algorithms such as fruit fly optimization algorithm (FOA) [16] have been applied to BPNN optimization. FOA is a global optimization algorithm established by simulating the foraging behavior of the fruit flies, and has been proven effective in parameter optimization [17–19]. However, proper initialization parameters of FOA should be determined; meanwhile, the flight distance of individual fruit fly is usually fixed and the searching direction is blind, resulting in degradation of the probability diversity of the FOA searching [20–22]. To address this issue, an improved fruit fly optimization algorithm (IFOA) is developed, and the IFOA optimized BPNN is proposed to improve the modeling capability for the MRD.

The reminders of this study are organized as follows. In section 2, a literature review is performed. In section 3, the proposed IFOA-BPNN surrogate model is introduced. In section 4, the damping characteristics of the MRD are experimentally described. In section 5, the surrogate model of the MRD is established and the modeling accuracy is analyzed. Conclusions and future work are summarized in section 6.

## 2. Related works

This section summarizes current researches in the field of MRD dynamic modeling and the improvement of FOA.

### 2.1. Dynamic modeling of MRD

Many investigations have been performed to model the nonlinear hysteretic characteristics of MRDs. Yu *et al* [23] divided the typical hysteresis loop into two curves, namely one backbone curve and one branch curve, the MRD dynamic model was simplified by capturing the characteristics of these two curves using exponential family function. Krauze *et al* [24] presented a new approach to establish the force–velocity characteristics model of the MRD. The model was able to simulate the hysteretic behavior using all-pass delay filters located in the velocity dedicated signal path, and could accurately reflect the MRD dynamic characteristics. Choi *et al* [25] proposed a hysteresis MRD model and the model accuracy was experimentally verified. Seong *et al* [26] established a Preisach hysteresis model for MRDs, and the first-order descending curves were experimentally identified. Subsequently, a feedforward hysteretic compensator associated with the biviscous model and inverse Bingham model was proposed to control the damping force. Domínguez *et al* [27] took the effect of each individual term of the Bouc–Wen model over the hysteretic loop into consideration, and established the dynamic model for MRD. Domínguez-González *et al* [28] proposed a new practical MRD model, which considered the displacement, velocity, acceleration and current as input variables, meanwhile, the hysteresis damping forces predicted by the proposed model were experimentally validated. However, modeling the nonlinear hysteresis of MRDs is a still challenge. Traditional analytical and experimental models are usually applicable to specific research objectives; and once the operation situations change the calculation accuracy of these models would significantly decay. AI and machine learning provide an effective alternative to model the MRD dynamics. Khalid *et al* [29] studied a small scale MRD model with a valve mechanism using dynamic regression neural network. Ni *et al* [30] established a nonlinear MRD dynamic model by a Bayesian inference framework. Nguyen *et al* [31] used an adaptive neural fuzzy reasoning system to establish the MRD dynamic model. Ayala *et al* [32] proposed a procedure for input selection and parameter estimation based on the radial basis functions neural networks to establish the MRD dynamic model. Imaduddin *et al* [33] developed a new parametric modeling approach based on the LuGre friction operator to reduce the number of involved parameters when modeling the MRD. Hemanth *et al* [34] established the mathematic MRD model based on the Boolean operation. Zhao *et al* [35] proposed a sigmoid modeling method to present the Stribeck effect of the MRD, and experimentally verified that the model can predict the damping forces.

### 2.2. Improvement of FOA

FOA has been found in many applications. Niu *et al* [36] optimized the FOA based on differential evolution (DFOA) and verified that the DFOA possessed strong global search capability and convergence stability. Liu *et al* [37] improved FOA using the cloud model algorithm. Xu *et al* [38] modified the flying range of FOA and showed the ability of avoiding local optimum for individual fruit fly using simulations and experiments. Han *et al* [39] proposed a new optimization algorithm based on FOA with

trend search and coevolution, and experimentally verified that the proposed algorithm had better precision and convergence speed. Lei *et al* [40] developed a FOA-based clustering algorithm to identify dynamic protein complexes by combining FOA and gene expression profiles. Zheng *et al* [41] proposed a knowledge-guided fruit fly optimization algorithm (KGFOA) and showed that KGFOA was more effective than FOA in solving the dual-resource constrained flexible job-shop scheduling problem.

### 2.3. Discussion

Literature has reported many dynamic models to improve the modeling accuracy of MRDs using AI-based techniques. However, several issues still need to be addressed. Firstly, the parameters of artificial neural networks such as a BPNN need to be optimized to improve the precision for modeling the hysteretic behavior of MRDs. FOA is able to optimize the neural network parameters to establish the MRD surrogate model while very limited work has been done for this purpose. Secondly, an AI surrogate model requires a large amount of training datasets to perform the knowledge learning; hence, an MRD testing platform is a must to generate reliable datasets of the MRD dynamics in different operation conditions. In order to bridge these research gaps in MRD dynamic modeling, an IFOA optimized BPNN is proposed and an MRD testing platform is developed to produce the required datasets for training the IFOA-BPNN model.

## 3. The proposed method

This section describes the proposed IFOA-BPNN method for modeling the MRD dynamics.

### 3.1. BPNN

BPNN is a multilayer feedforward neural network based on error inverse propagation algorithm, which is proposed in 1986 [42]. It consists of an input/output layer and an implicit layer. BPNN learn and save the corresponding relationship between the input and output data, when their mathematical relationship has not been accurately determined. The data samples obtain the output values of the network characteristics by training the neural network, the error between the output of network and original data is considered as a feedback signal of fixed network, which travels in the opposite direction of data transmission, the network is corrected according to error gradient descent method to continuously reduce the sum of error squares of network training [43]. The structure diagram of a three-layer BPNN is shown in figure 1.

The input of node  $i$  in the hidden layer:

$$net_i = \sum_{j=1}^m w_{ij}x_j + \theta_i \quad (1)$$

The output of node  $i$  in the hidden layer:

$$y_i = \phi(net_i) = \phi\left(\sum_{j=1}^m w_{ij}x_j + \theta_i\right) \quad (2)$$

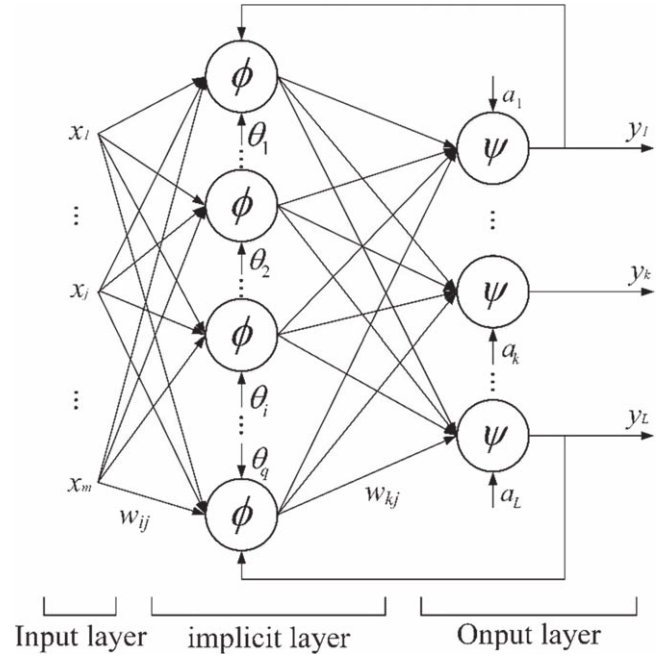


Figure 1. Structure diagram of three-layer BPNN.

The input of node  $k$  in the output layer:

$$net_k = \sum_{i=1}^q w_{ki} \phi\left(\sum_{j=1}^m w_{ij}x_j + \theta_i\right) + a_k \quad (3)$$

The output of node  $k$  of the hidden layer:

$$y_k = \psi\left[\sum_{i=1}^q w_{ki} \phi\left(\sum_{j=1}^m w_{ij}x_j + \theta_i\right) + a_k\right] \quad (4)$$

where  $w_{ij}$  and  $\theta_i$  are the connection weight and threshold of input neurons,  $\phi$  is the transfer function of implicit layer,  $\psi$  is the transfer function of output layer,  $w_{kj}$  and  $a_k$  are the connection weights and thresholds of network layer neurons,  $y_k$  is the output of node  $k$  in output layer.

Assuming that the input of the network is  $P_m$  and the target vector of the network is  $T_L$ , the error value of the feedback can be expressed as  $e_k = T_k^p - y_k^p$ . Then the obtained feedback signal is  $e = (e_1, e_2, \dots, e_p)$ . The correction matrix of weight and threshold is shown in equation (5):

$$\left\{ \begin{array}{l} \Delta w_{ki} = \eta \sum_{p=1}^P \sum_{k=1}^L (T_k^p - y_k^p) \cdot \psi'(net_k) \cdot \theta_i \\ \Delta a_k = \eta \sum_{p=1}^P \sum_{k=1}^L (T_k^p - y_k^p) \cdot \psi'(net_k) \\ \Delta w_{ji} = \eta \sum_{p=1}^P \sum_{k=1}^L (T_k^p - y_k^p) \cdot \psi'(net_k) \cdot w_{ki} \cdot \phi'(net_i) \cdot x_j \\ \Delta \theta_i = \eta \sum_{p=1}^P \sum_{k=1}^L (T_k^p - y_k^p) \cdot \psi'(net_k) \cdot w_{ki} \cdot \phi'(net_i) \end{array} \right. \quad (5)$$

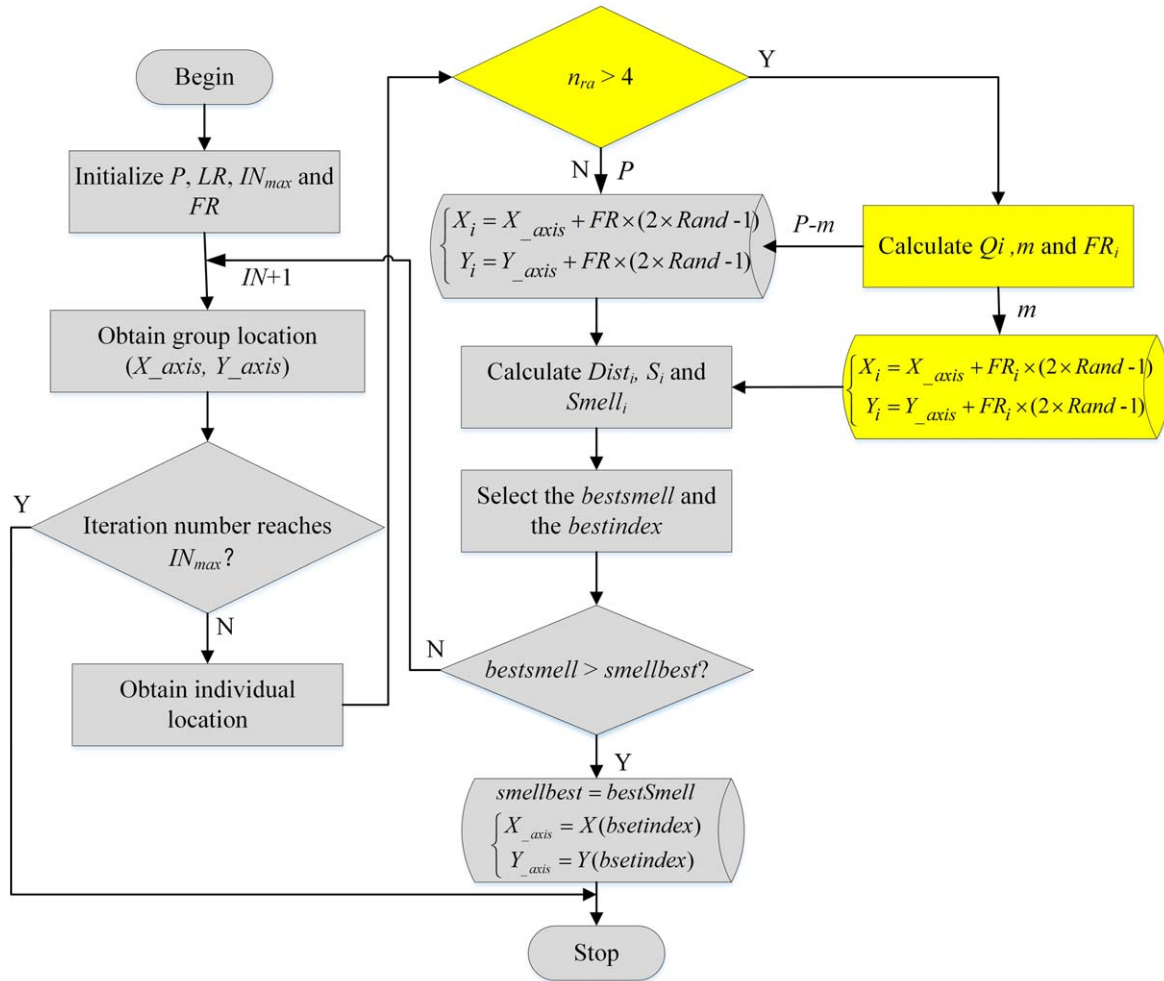


Figure 2. Flowchart of the IFOA.

Table 1. The optimal solution of the four test functions.

Algorithm	Ackely	Rastrigin	Griewank	Matyas
FOA	0.039 614	3.741 703	0.010 74	2.90E-06
GA	0.040 588	0.0068	0.003 745	0.001303
IFOA	0.000 698	0.001 12	0.001 252	2.46E-06

Equation (5) indicates that the weight and threshold values are corrected along the opposite direction of the data flow by the correction matrix, so as to achieve the aim of reducing the output error.

### 3.2. The FOA and proposed IFOA

During the process of foraging, the fruit fly determines the location of the food according to the smell, the other individuals gather around the food through the connections between them. The implementation of FOA can be summarized as following steps [37].

**Step 1.** The population amount ( $P$ ), the maximum iteration number ( $IN_{max}$ ), the flying distance range ( $FR$ ), the group

location range and the initial location ( $X_{axis}, Y_{axis}$ ) of fruit fly population are determined.

**Step 2.** Calculate the random flight direction and distance to search for food of the fruit fly individual.

$$\begin{cases} X_i = X_{axis} + 2 \times FR \times Rand_i - FR \\ Y_i = Y_{axis} + 2 \times FR \times Rand_i - FR \end{cases} \quad (6)$$

**Step 3.** Calculate the distance between the fruit fly individual and the origin, and then calculate the flavor concentration parameter which is the reciprocal of the distance.

$$\text{Distance} : Dist_i = \sqrt{X_i^2 + Y_i^2} \quad (7)$$

$$\text{Concentration parameter} : S_i = 1 / Dist_i. \quad (8)$$

**Step 4.** Substitute  $S_i$  into the fitness function, calculate the value of flavor concentration function  $Smell_i$  and find out the best flavor concentration in the fruit fly population. The

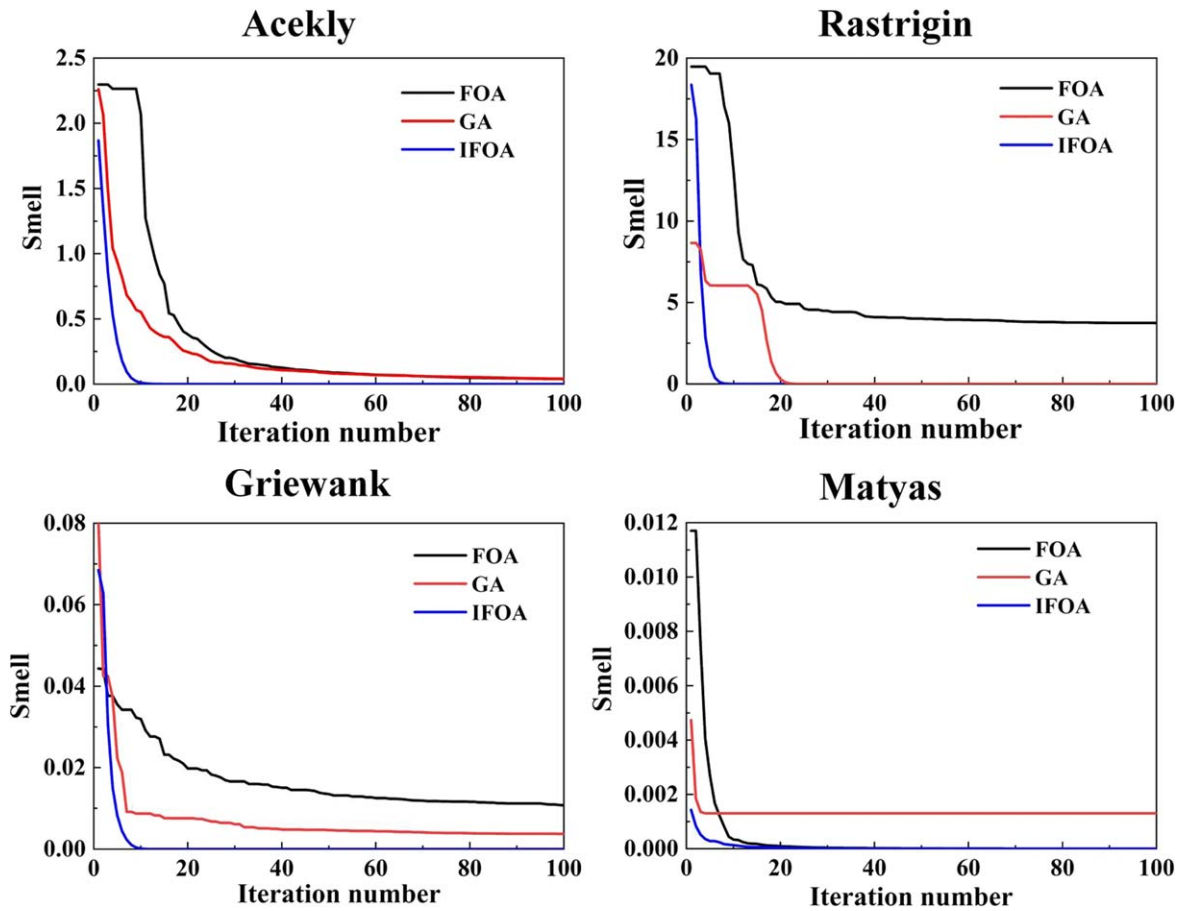


Figure 3. The convergence curves of the test functions.

minimum value is taken as the best flavor concentration in this paper.

$$Smell_i = Function(S_i) \tag{9}$$

$$[best\ Smell, bestindex] = \min(Smell). \tag{10}$$

**Step 5.** Obtain the best flavor value and the coordinates of  $(X_{axis}, Y_{axis})$ , the fruit fly population flies to that location through vision at this point.

$$smellbest = bestSmell \tag{11}$$

$$\begin{cases} X_{axis} = X(bsetindex) \\ Y_{axis} = Y(bsetindex) \end{cases} \tag{12}$$

**Step 6.** When the smell concentration reaches the preset precision value or the iteration number reaches the maximal  $IN_{max}$ , the searching stops. Otherwise, repeat Steps 2–4.

It can be obtained from steps 1–6 that the flight distance of individual fruit fly in FOA is within a fixed interval and the searching direction is blind, the probability of falling into local optimum greatly increases, and then some individual fruit flies cannot escape from the local optimum. Furthermore,

the convergence precision is reduced in the later iteration, which severely limits the search capability of FOA.

In order to improve the global search capability of FOA, An IFOA is proposed in this paper. In IFOA, a heuristic factor  $Q_i$  was added into the FOA, which could push some individuals escape from the local optimal position and searching for the next optimal position with a greater searching distance. The heuristic factor  $Q_i$  is presented as follows:

$$Q_i = \begin{cases} \frac{n_{ra} \times \eta_i \times Smell_b}{\frac{1}{P} \sum_{k=1}^P Smell_i}, & n_{ra} \geq 5 \\ 0, & 0 \leq n_{ra} \leq 5 \end{cases} \tag{13}$$

$$m = \begin{cases} P \times Q_i, & 0 \leq Q_i \leq 1 \\ P, & 0 \leq n_{ra} \leq 5 \end{cases} \tag{14}$$

$$FR_i = \frac{FR + 1}{2} \times \left(1 - \frac{IN}{IN_{max}}\right) + \frac{(FR + 1)^{Int\left(\frac{1}{1.5-Q_i}\right)}}{2}, \tag{15}$$

where  $Smell_b$  is the minimum flavor concentration in fruit fly population,  $n_{ra}$  is a coefficient which make the optimal value of fruit fly population is constant,  $\eta_i$  is the number of fruit fly individual within  $(Smell_b, a.Smell_b)$ ,  $a$  is a coefficient that determines the range of flavor concentrations of fruit flies,  $m$  is the number of fruit fly individual escaped from the local optimal



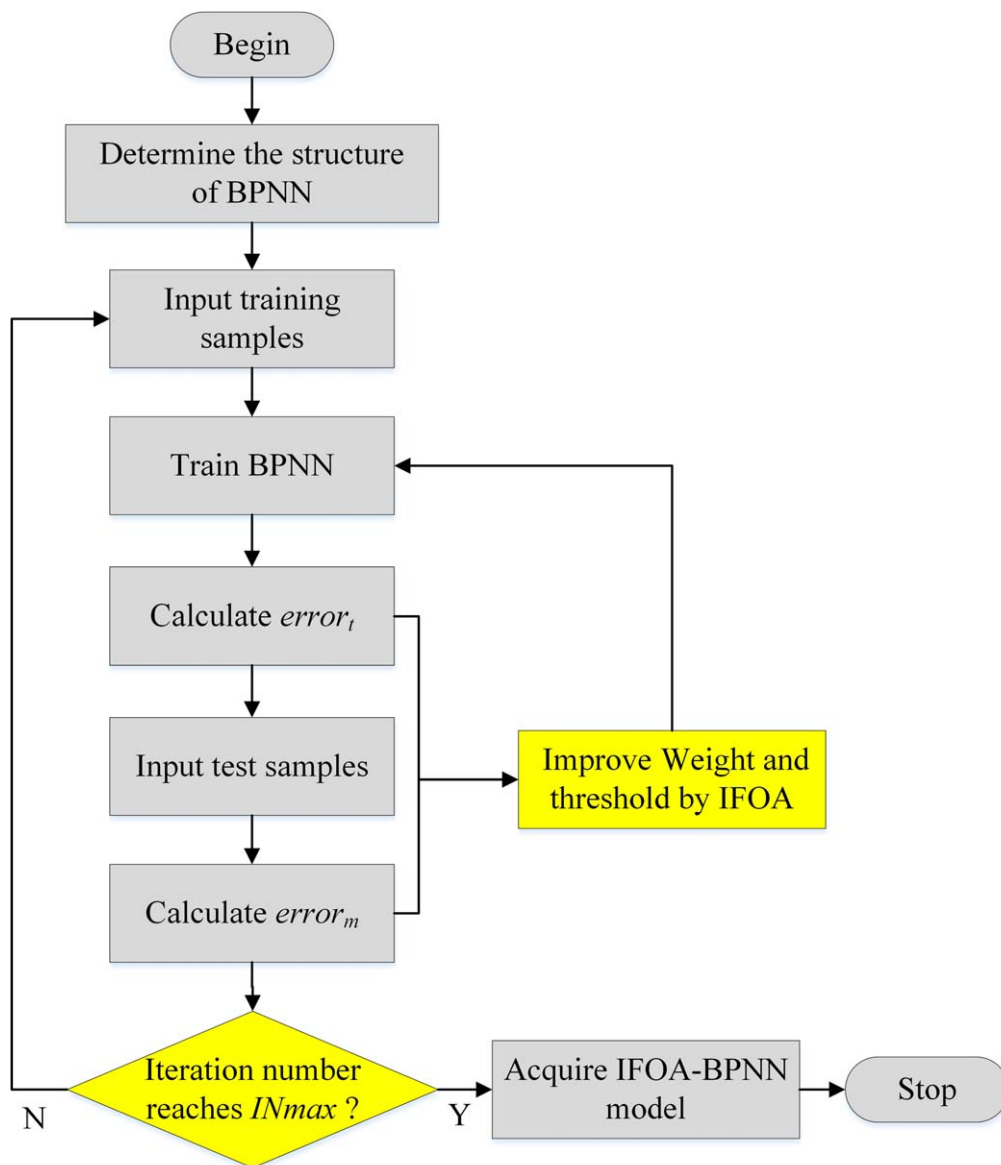


Figure 4. The modeling process of IFOA-BPNN.

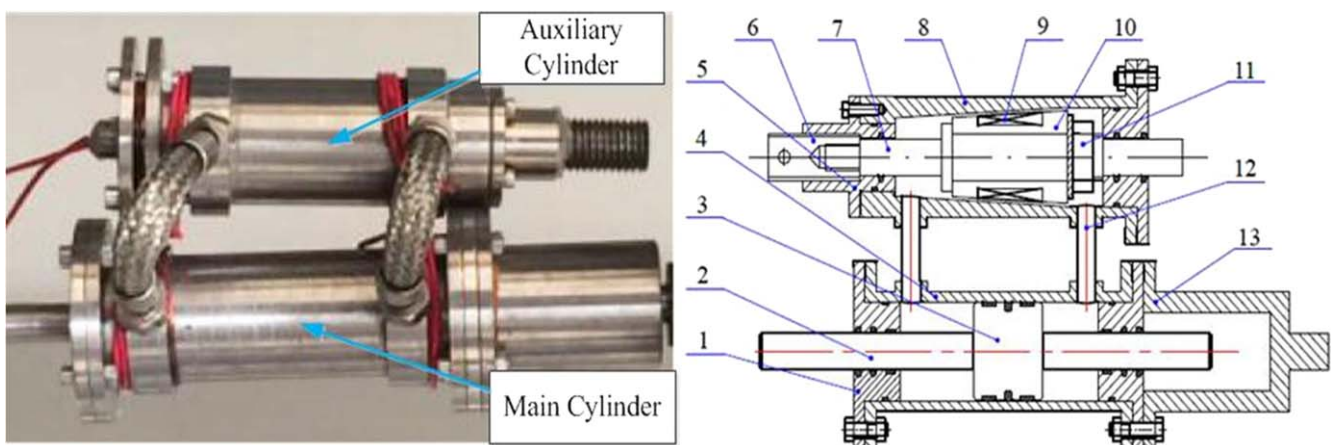


Figure 5. The physical figure and structure diagram of MRD. (1)–(3): left end cover of main cylinder, piston rod of main cylinder, piston of main cylinder, cylinder of main cylinder, left end cover of auxiliary cylinder, connector of auxiliary cylinder, piston rod of auxiliary cylinder, cylinder of auxiliary cylinder, coil, piston of auxiliary cylinder, hexagon nut, backflow port and right end cover of main cylinder, respectively.

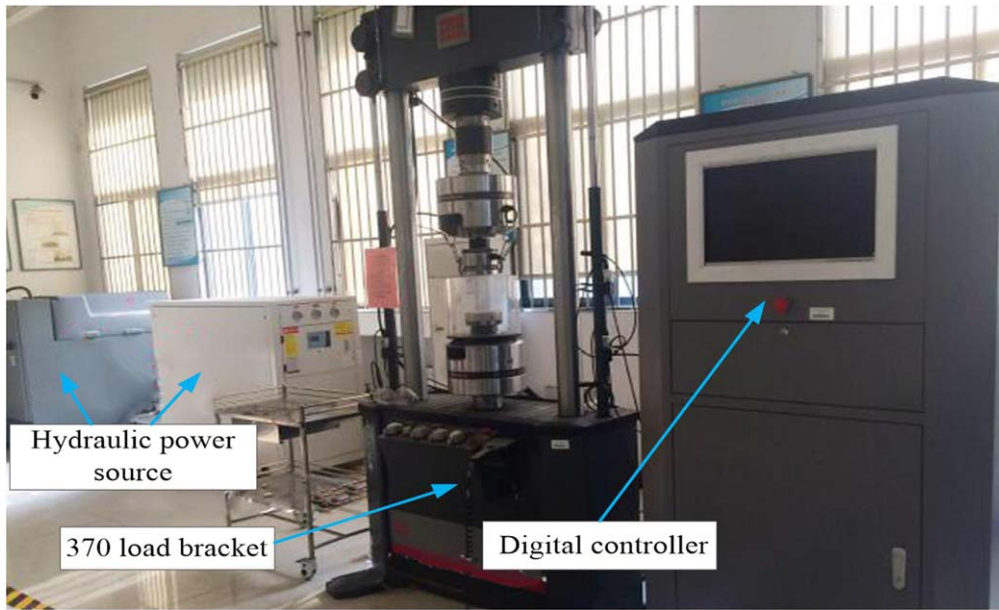


Figure 6. MTS Landmark 370.50 test system.

Table 2. Main technical parameters of MTS Landmark 370.50 test system.

Parameters	Values
Static test force (kN)	±500, precision ≥ ±0.5%
Dynamic test force (kN)	±500, precision ≥ ±0.5%
Maximum frequency (Hz)	80
Sampling frequency range (kHz)	0–122
Maximum amplitude (mm)	±625

Table 3. Main technical parameters of DP811A programmable power.

Parameters	Values
Voltage range (V)	0–40
Current range (A)	0–5
Transient response time (μs)	<50
Resolution (mV mA <sup>-1</sup> )	1/0.5

position,  $FR_i$  is the searching distance of fruit fly individuals which is updated by the heuristic factor,  $IN$  is the current iteration number. The flow chart of IFOA is shown in figure 2.

In order to verify the search capability of the IFOA, four tests were conducted using four popular functions (i.e., Ackely, Rastrigin, Griewank and Matyas). The convergence trend and optimization precision of the tests were compared using FOA, genetic algorithm (GA) and IFOA. Table 1 shows the optimal solutions of the four test functions. The initialization conditions were the same for the three algorithms; that is, the population quantity was 30 and the iteration number was 100. Figure 3 shows the convergence curves of the test functions.

As can be seen in table 1, the smallest optimal solution of the four test functions is produced by the proposed IFOA method. Figure 3 shows that the proposed IFOA has a faster convergence speed and a higher convergence precision than

the other two methods, which indicates that the search capability of the IFOA is better than original FOA and GA.

### 3.3. IFOA-BPNN

The basic principle for using the IFOA to optimize the BPNN is that the direction and distance of fruit fly individual are regarded as the weight and threshold of the BPNN, the fitness function is established by using the training error and test error of BPNN, which is also used to evaluate the position information of fruit fly individual. The flowchart of IFOA-BPNN is shown in figure 4, the fitness function is presented as follows:

$$f = \delta \times error_t + (1 - \delta) \times error_m, \delta \in (0, 1), \quad (16)$$

where  $error_t$  and  $error_m$  are the training error and test error of the BPNN, respectively.  $\delta$  is the weight value between the training error and test error. The mean square error value is selected as the evaluation index, which is shown as follows:

$$error = \frac{1}{K} \sum_{i=1}^K (x_i - \hat{x}_i)^2. \quad (17)$$

The implementation of IFOA-BPNN can be summarized as following steps.

**Step 1.** Initialize the BPNN; determine the number of neurons in the input layer, hidden layer and output layer of the BPNN, respectively; and then calculate the number of weights and thresholds according to the number of neurons in each layer.

**Step 2.** Each weight and threshold is considered as a fruit fly individual, and initialize their position.

**Step 3.** Assign values to random direction and distance for each weight and threshold by random function, which are in searching global optimal value.

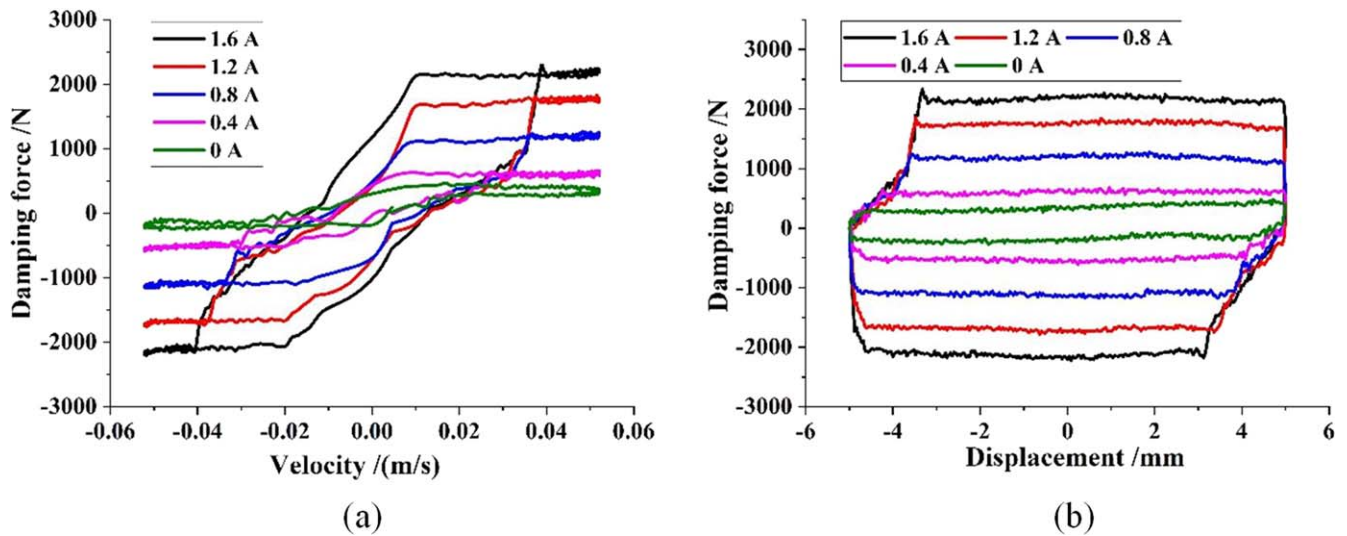


**Figure 7.** The damping characteristic curves: (a) damping force–velocity and (b) damping force–displacement when the amplitude of MRD is 5 mm and the excitation frequency is 1.66 Hz.

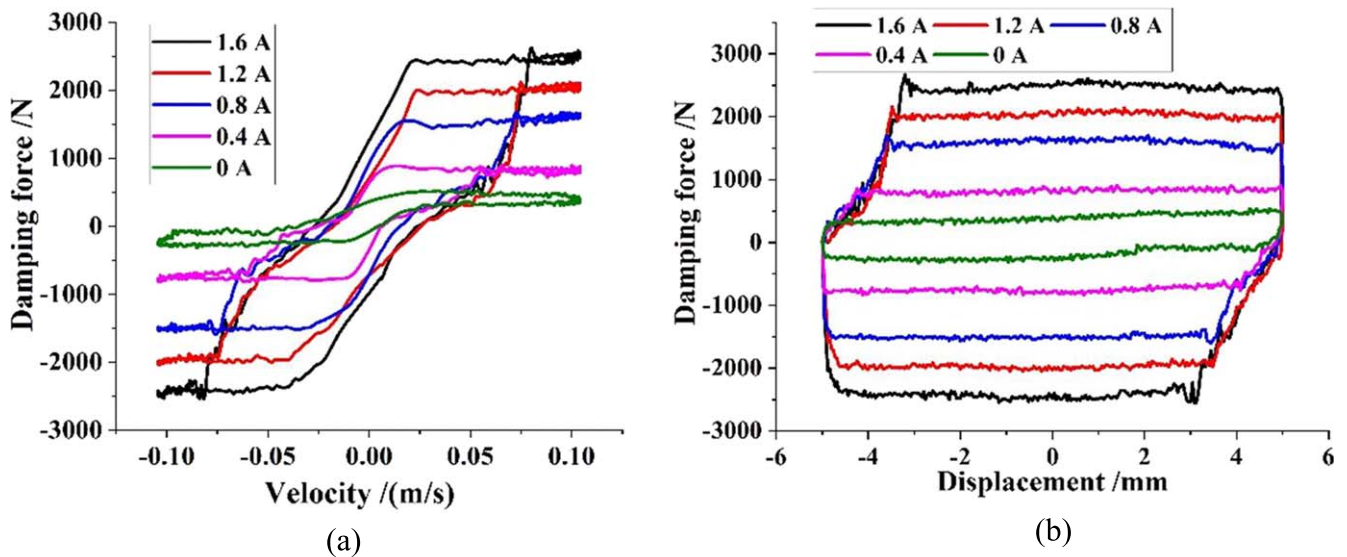


**Figure 8.** The damping characteristic curves: (a) damping force–velocity and (b) damping force–displacement when the amplitude of MRD is 5 mm and the excitation frequency is 3.32 Hz.

**Step 4.** Calculate the distance  $D$  between the individual and origin, and then calculate the flavor concentration judgment value, which is the reciprocal of  $D$ .

**Step 5.** The training data are used to train the BPNN, and the test data are substituted into the trained BPNN for verification.

**Step 6.** Substitute flavor concentration judgment value in Step 4 into the fitness function to obtain the minimum value, and record the corresponding weights and thresholds.

**Step 7.** Optimize the value of fitness function by using the obtained minimum value in Step 6, and then store the coordinates of weights and thresholds.

**Step 8.** Repeat steps 3 and 6, and determine whether the fitness function is better than the previous generation. If so, perform step 7.

**Step 9.** The optimal weights and thresholds obtained in the iteration process are substituted into the BPNN for modeling.

## 4. MRD dynamics testing and analysis

### 4.1. A new MRD testing platform

This study designed and fabricated a new MRD, as shown in figure 5. This new MRD includes a main cylinder and an auxiliary cylinder. The main cylinder is used to bear external

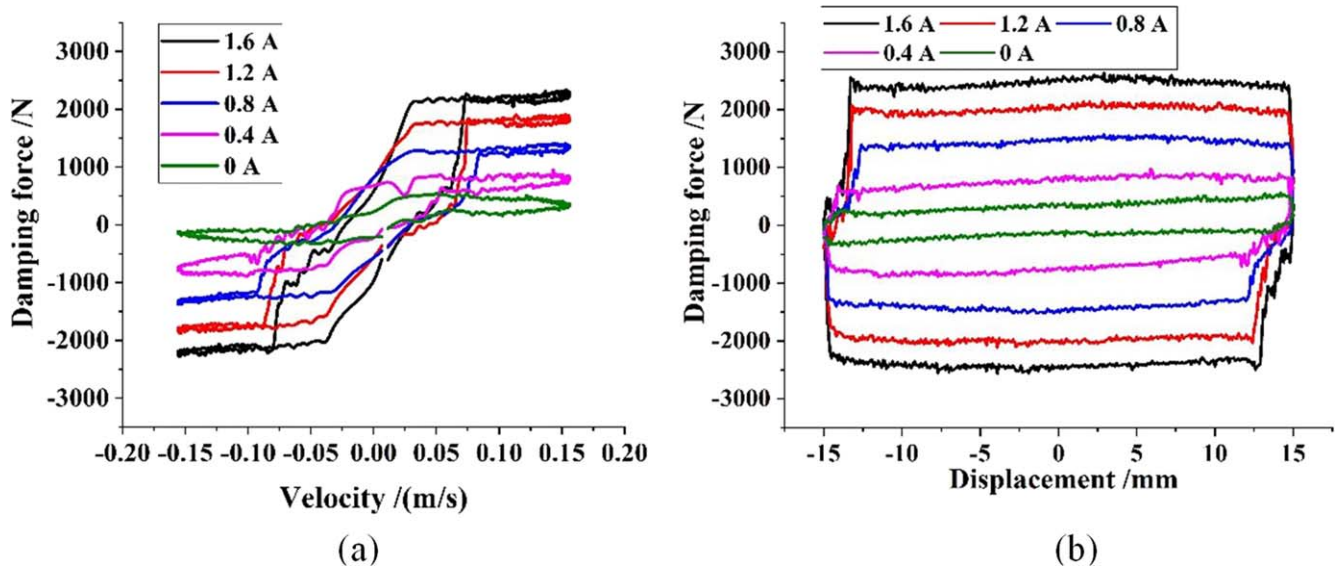


**Figure 9.** The damping characteristic curves: (a) damping force–velocity and (b) damping force–displacement when the amplitude of MRD is 15 mm and the excitation frequency is 1.66 Hz.

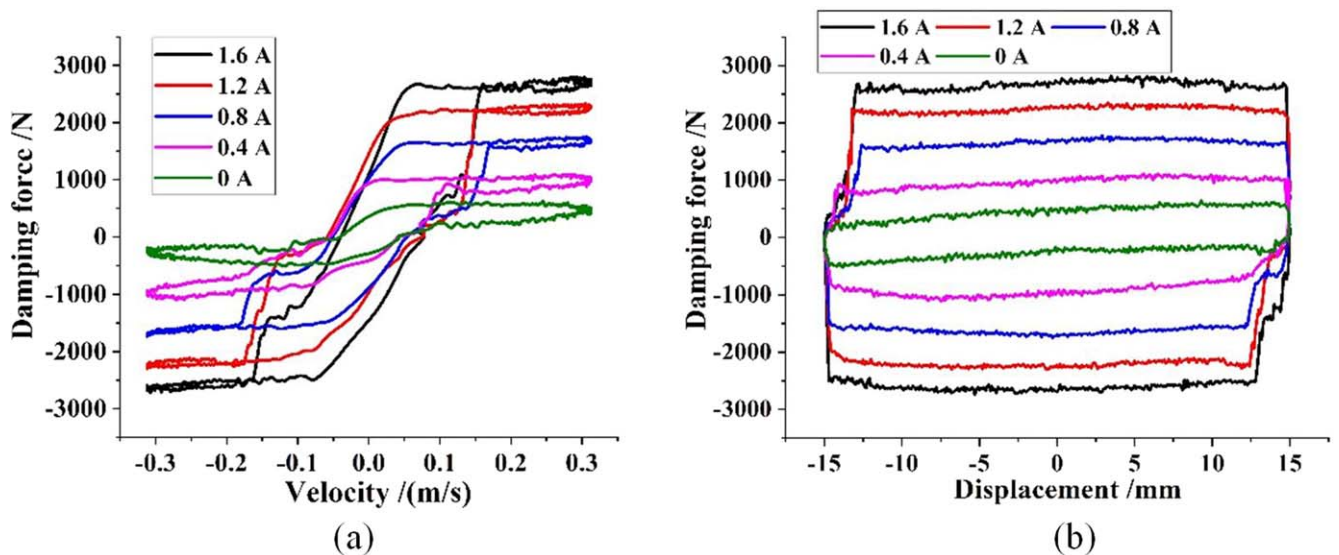


**Figure 10.** The damping characteristic curves: (a) damping force–velocity and (b) damping force–displacement when the amplitude of MRD is 15 mm and excitation frequency is 3.32 Hz.

loads and the auxiliary cylinder is used to control the damping forces. The excitation coil is wound around the piston of auxiliary cylinder, and a damping channel is formed between the piston and the cylinder of auxiliary cylinder. When a force is applied on the piston rod of main cylinder, the piston of main cylinder will be driven to move, then the magnetorheological fluid (MRF) on one side of the main cylinder will enter the auxiliary cylinder through the backflow port under the action of pressure. In this process, the MRF in auxiliary cylinder will move from one end to another end through damping channel, meanwhile, the rheological effect of MRF is exhibited under the action of magnetic field, due to the shear yield stress of MRF can be controlled in real-time by

adjusting the current intensity, the continuous control of the piston rod of main cylinder could be realized. The piston and cylinder of auxiliary cylinder are designed with an inclined plane, which has an angle of  $3^\circ$  with the axial direction. The piston rod of the auxiliary cylinder is connected with the left end cover by thread, the axial position of the piston of the auxiliary cylinder can be adjusted so as to control the size of damping channel by rotating the piston rod. The piston and cylinder of auxiliary cylinder are made of steel 45, the end cover of auxiliary cylinder is made of stainless steel. The length and diameters at both ends of piston of auxiliary cylinder are 110 mm, 36 mm and 25 mm, respectively. The damping channel clearance is adjustable within 0–2 mm.

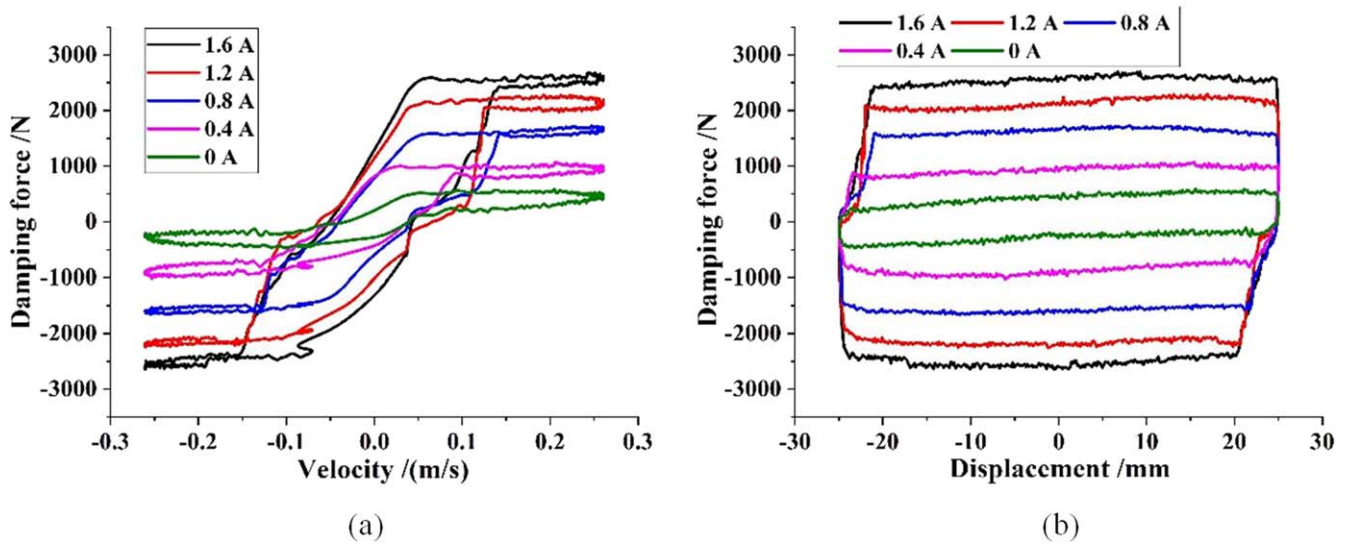


**Figure 11.** The damping characteristic curves: (a) damping force–velocity and (b) damping force–displacement when the amplitude of MRD is 25 mm and excitation frequency is 1.66 Hz.

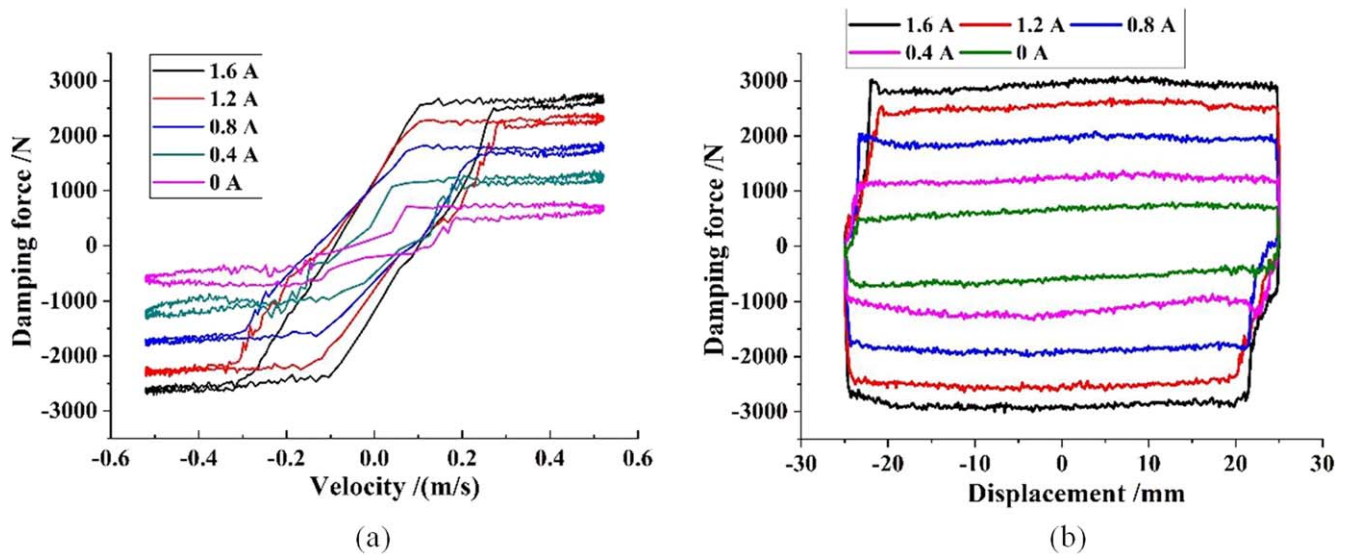


**Figure 12.** The damping characteristic curves: (a) damping force–velocity and (b) damping force–displacement when the amplitude of MRD is 25 mm and excitation frequency is 3.32 Hz.

The damping characteristics of the MRD were obtained by the load test system (MTS Landmark 370.50), as shown in figure 6, which consists of a 370 load bracket, a hydraulic power source and a digital controller (FlexTest 60). The main technical parameters of the system are shown in table 2. The programmable current source (DP811A) was used to provide current for the excitation coil; the relevant technical parameters are shown in table 3.

The MRF-250 was used in this study. It is comprised of soft magnetic carbonyl iron particles (average diameter: 8  $\mu\text{m}$ , density: 7.86  $\text{g cm}^{-3}$ ; Beijing DK Nano Technology Co., Ltd), dimethyl silicone oil (viscosity: 100 cSt at 25  $^{\circ}\text{C}$ , density: 0.965  $\text{g cm}^{-3}$ ; Shin-Etsu, Japan), sodium dodecyl benzene sulfonate, oleic acid (purity 90%), graphite, and

diatomite powder. The zero field viscosity, saturation yield stress and working temperature of MRF-250 are 242.5 mPa s, 55.25 kPa and  $-40^{\circ}\text{C}$  to  $150^{\circ}\text{C}$ , respectively.

#### 4.2. MRD dynamics analysis

The damping characteristics of the MRD were tested under harmonic excitations. In the experiments, the amplitudes of the MRD were 5 mm, 15 mm and 25 mm, respectively; the excitation frequencies were 1.66 Hz and 3.32 Hz, respectively; the excitation currents were 0 A, 0.4 A, 0.8 A, 1.2 A and 1.6 A, respectively; and the sampling frequency was 500 Hz. The piston was forced to return to the original position, and the power supply was turned off to avoid the

**Table 4.** Training sample data.

Serial No.	Current/A	Speed/(m s <sup>-1</sup> )	Amplitude/mm	Frequency/(Hz)	Force/N	Normalization				
1	0	0.004 54	5	1.66	18.44	0	0.004 54	0.1	0.5	0.005 269
2	0	0.0096	5	1.66	155.4	0	0.0096	0.1	0.5	0.0444
3	0	0.011 12	5	1.66	106.47	0	0.011 12	0.1	0.5	0.030 42
⋮	⋮	⋮	⋮	⋮	⋮	⋮	⋮	⋮	⋮	⋮
803	0	0.011 51	15	1.66	-64.71	0	0.011 51	0.3	0.5	-0.018 49
804	0	0.019 47	15	1.66	65.85	0	0.019 47	0.3	0.5	0.018 814
805	0	0.032 45	15	1.66	51.8	0	0.032 45	0.3	0.5	0.0148
⋮	⋮	⋮	⋮	⋮	⋮	⋮	⋮	⋮	⋮	⋮
2723	0	-0.103 72	25	3.32	-442.376	0	-0.103 72	0.5	1	-0.126 39
2724	0	-0.076 03	25	3.32	-351.185	0	-0.076 03	0.5	1	-0.100 34
2725	0	0.055 43	25	3.32	-156.014	0	0.055 43	0.5	1	-0.044 58
⋮	⋮	⋮	⋮	⋮	⋮	⋮	⋮	⋮	⋮	⋮
13622	1.6	-0.103 72	25	3.32	-2525.46	0.8	-0.103 72	0.5	1	-0.721 56
13623	1.6	-0.076 03	25	3.32	-1882.35	0.8	-0.076 03	0.5	1	-0.537 82
13624	1.6	-0.023 02	25	3.32	-1386.3	0.8	-0.023 02	0.5	1	-0.396 09

**Table 5.** Testing sample data.

Serial No.	Current/A	Speed/(m s <sup>-1</sup> )	Amplitude/mm	Frequency/(Hz)	Force/N	Normalization				
1	0	0.013 08	5	1.66	238.64	0	0.013 08	0.1	0.5	0.068 183
2	0	0.019 42	5	1.66	268.73	0	0.019 42	0.1	0.5	0.076 78
3	0	0.023 97	5	1.66	298.35	0	0.023 97	0.1	0.5	0.085 243
⋮	⋮	⋮	⋮	⋮	⋮	⋮	⋮	⋮	⋮	⋮
201	0	0.026 66	15	1.66	88.67	0	0.026 66	0.3	0.5	0.025 334
202	0	0.0471	15	1.66	132.57	0	0.0471	0.3	0.5	0.037 877
203	0	0.061 14	15	1.66	234.42	0	0.061 14	0.3	0.5	0.066 977
⋮	⋮	⋮	⋮	⋮	⋮	⋮	⋮	⋮	⋮	⋮
679	0	-0.195 93	25	3.32	-750.66	0	-0.195 93	0.5	1	-0.214 47
680	0	-0.145 95	25	3.32	-615.45	0	-0.145 95	0.5	1	-0.175 84
681	0	0.023 02	25	3.32	-223.295	0	0.023 02	0.5	1	-0.0638
⋮	⋮	⋮	⋮	⋮	⋮	⋮	⋮	⋮	⋮	⋮
3404	1.6	-0.187 13	25	3.32	-2602.28	0.8	-0.187 13	0.5	1	-0.743 51
3405	1.6	-0.133 46	25	3.32	-2741.34	0.8	-0.133 46	0.5	1	-0.783 24
3406	1.6	0.055 43	25	3.32	-488.586	0.8	0.055 43	0.5	1	-0.1396

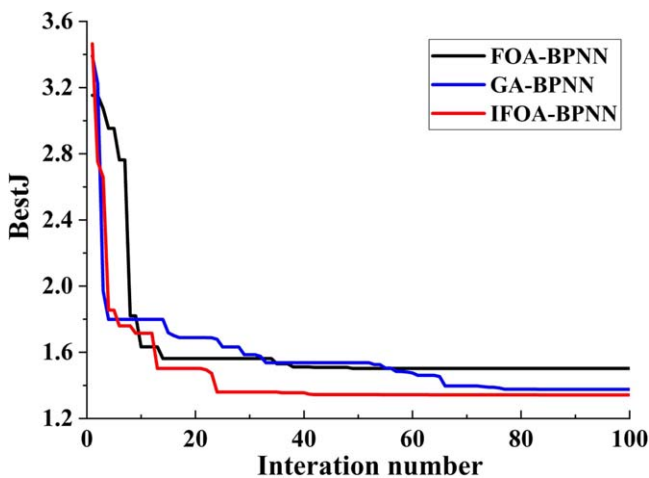


**Figure 13.** Iteration curves for fitness.

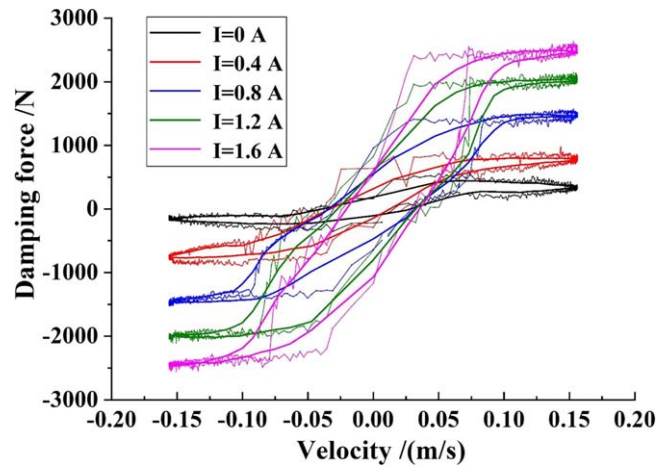


**Figure 14.** The experimental curves and modeling curves of damping force when the amplitude of MRD is 15 mm and excitation frequency is 1.16 Hz.

**Table 6.** Training error and test error.

Modeling method	BPNN	FOA-BPNN	GA-BPNN	IFOA-BPNN
Training error	3.157	2.943	2.683	2.529
Test error	1.116	1.053	0.943	0.895

residue effect when one test period was complete. The time interval for each test was 1 min. Figures 7–12 show the damping characteristic curves of the MRD.

Figures 7–12 indicate that the damping forces change rapidly with the variation of velocity in the low speed region; moreover, the significant hysteresis is found in this region. The reason for this phenomenon is that a certain time is taken to generate the rheological effect of MRF, furthermore, an amount of air exists in the MRF, which results in the compression of MRF. In the high speed region, the damping force is basically kept in a steady state and the hysteresis effect almost disappears. It can be seen from the figures 7–12 that the damping force increases with the excitation current when the velocity and displacement are in a constant state. Although there is hysteresis in the damping force, it still reaches the normal working state when the piston is not in the extreme position. Once the piston reaches the extreme position, the damping force rapidly attenuates to the zero state. When the amplitude of damper is 25 mm, excitation frequency is 3.32 Hz and the excitation current is 1.6 A, the damping force reaches 3064.97 N. The large oscillation exists in the test results is due to the error of sensor, meanwhile, the diameter of the magnetic particle is not uniform, which results in the difference in rheological effect.

## 5. Dynamic modeling using IFOA-BPNN

In this paper, BPNN, GA-BPNN [44], FOA-BPNN and IFOA-BPNN were employed to establish the MRD surrogate models, respectively. The performance of the AI surrogate models was compared. The training data in table 4 is used to obtain the network model, and the test data in table 5 is used to test the performance of network. In order to avoid erroneous datasets, it is necessary to unify the samples in the training and test by normalization processing. The training error, learning rate and training times were 0.1, 0.01 and 1000, respectively. The function Logsig was used as activation function of the output layer, and function Tansig was used as a negative gradient descent momentum method to train the BPNN. The population quantity of fruit fly was 30 and the iteration number was 100.

Figure 13 shows the iteration curves for fitness during modeling time. It indicates that the FOA-BPNN, GA-BPNN and IFOA-BPNN are converged when the iteration number are 38, 77 and 42, respectively. When the calculations reach a steady state, the fitness values of FOA-BPNN, GA-BPNN and IFOA-BPNN are 1.54, 1.44 and 1.09, respectively, which indicate that the IFOA-BPNN has higher convergence

accuracy and faster convergence speed than FOA-BPNN and GA-BPNN, moreover, the IFOA-BPNN is better in searching.

Taking the experimental results of MRD dynamic characteristic as training and prediction samples. When the input variables of the network are amplitude, frequency and speed of excitation, current, the output variables are damping force. The positive model of MRD is identified based on IFOA-BPNN. When the input variables of the network are amplitude, frequency and speed of excitation, damping force, the output variables of the network is control current. The inverse model of damper is identified based on IFOA-BPNN. Figure 14 shows the variation curves of damping force and velocity in different currents under the condition of amplitude is 15 mm and excitation frequency is 1.66 Hz, which includes the experimental results and the predicted results of IFOA-BPNN positive model. The thick and thin lines represent the experimental and the predicted results, respectively. It can be seen from the figure 14 that the model established by IFOA-BPNN accurately simulates the variation of damping force with the velocity and current, and the hysteresis behavior of MRD can be clearly exhibited.

Table 6 shows the training errors and test errors of BPNN, FOA-BPNN, GA-BPNN and IFOA-BPNN in the modeling process. In table 6, the training error of IFOA-BPNN decreases by 19.89%, 14.07% and 6.09%, and the test error of IFOA-BPNN decreases by 19.8%, 15.01% and 5.29% compared with other methods, which indicates that the modeling performance of IFOA-BPNN is superior to GA-BPNN, FOA-BPNN and BPNN.

In order to further verify the accuracy of IFOA-BPNN in modeling, 108 groups of test samples were extracted and substituted into the dynamic models in the states of current were 0 A, 0.8 A and 1.6 A, respectively. Figure 15 shows the test error rate of BPNN, FOA-BPNN, GA-BPNN and IFOA-BPNN. Figure 15 indicates test error rate is the smallest by using the method of IFOA-BPNN, which demonstrates that the accuracy of IFOA-BPNN in modeling is obviously higher than other methods. The large errors are found between sample 50 and sample 60, and the corresponding speed between the sample 50 and sample 60 are  $0.2 \text{ m s}^{-1}$ – $0.35 \text{ m s}^{-1}$  and  $-0.35 \text{ m s}^{-1}$  to  $-0.2 \text{ m s}^{-1}$ , which indicates that the modeling effects of BPNN, GA-BPNN, FOA-BPNN and IFOA-BPNN are poor in the transition zone, but the IFOA-BPNN is significantly better than others.

In order to research the relationship between modeling accuracy and current, average absolute error rates of the four modeling methods were tested when the currents were 0 A, 0.4 A, 0.8 A, 1.2 A and 1.6 A, respectively, the corresponding amplitude was 15 mm, and the excitation frequency was 3.32 Hz, as shown in figure 16. Figure 16 indicates that the modeling accuracy of BPNN are greatly improved by adding intelligent algorithms, and the modeling accuracy of IFOA-BPNN is better than other methods, moreover, the modeling accuracy increases with the current.

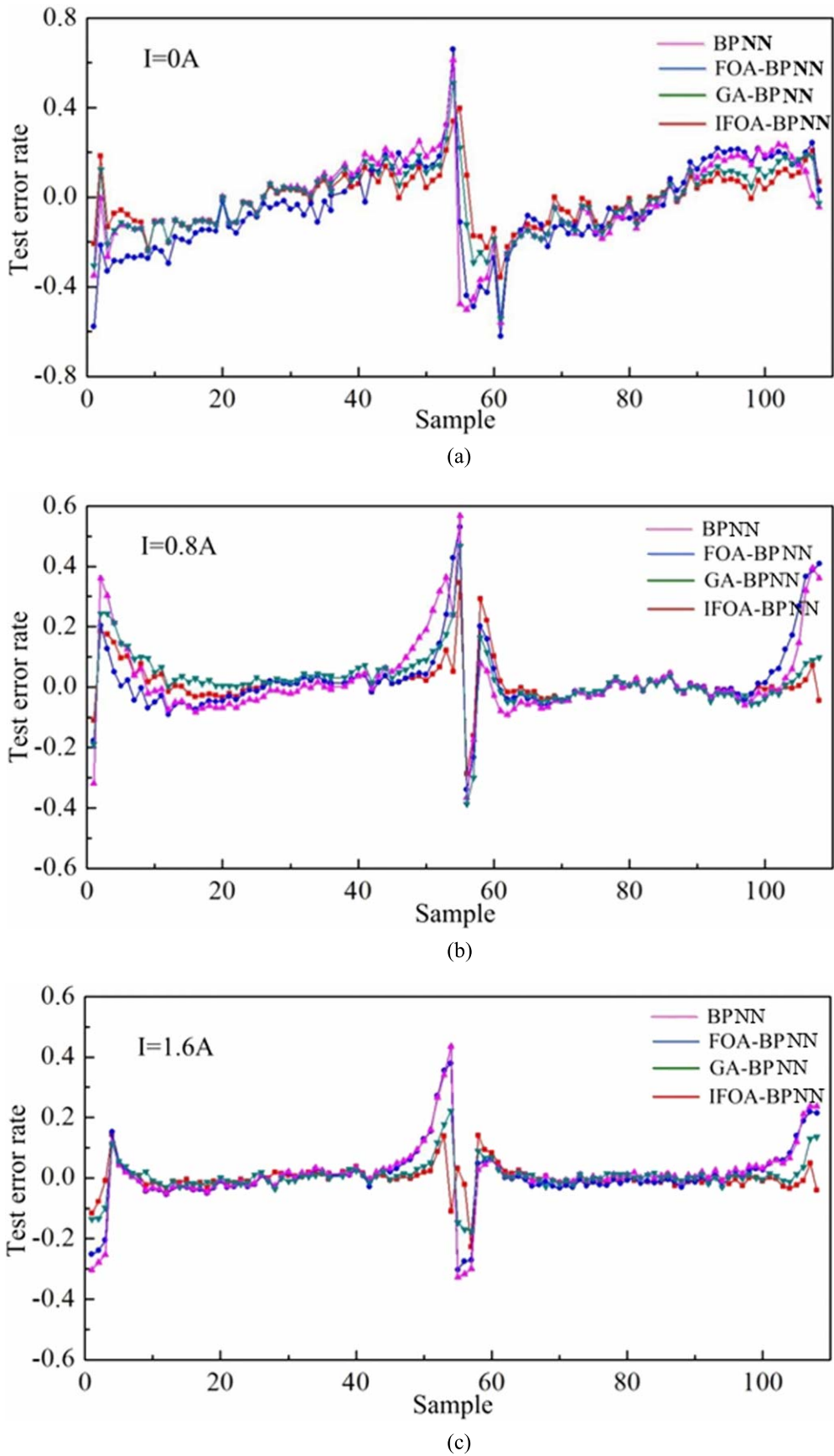
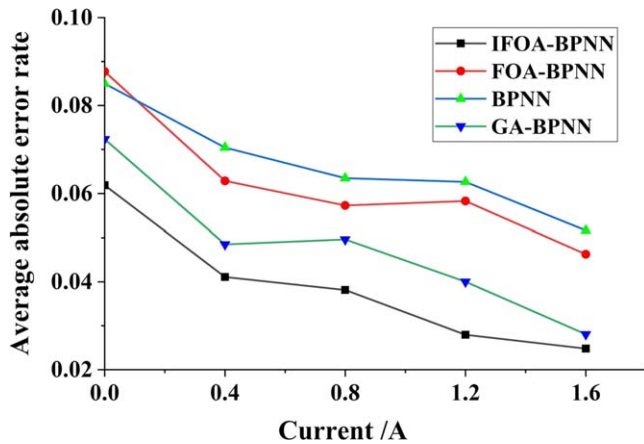


Figure 15. Test error rate of the four methods under the condition of the amplitude is 25 mm and excitation frequency is 3.32 Hz.





**Figure 16.** Relationship between current and average absolute error rate under the condition of the amplitude is 25 mm and excitation frequency is 3.32 Hz.

## 6. Conclusions and future work

With the aim to improve the modeling accuracy for a MRD, an IFOA-BPNN method was proposed. A new MRD testing platform was established to generate experimental datasets for the identification of modeling parameters. An IFOA-BPNN surrogate model was then established to represent the dynamics of the MRD. The performance of the IFOA-BPNN was compared with BPNN, FOA-BPNN and GA-BPNN in terms of modeling accuracy. The analysis results demonstrated that the modeling accuracy of IFOA-BPNN was satisfactory and was superior to its competitors.

Though the IFOA-BPNN is capable to improve the modeling accuracy of the MRD in this study, there are still some shortcomings need to be addressed. For example, the modeling error of IFOA-BPNN is still large in the transition zones of low speed and high speed. This issue will be solved in future study. Moreover, based on the IFOA-BPNN surrogate model, an optimal controller will be developed to remove hostile vibrations of the MRD-based semi-active seat suspension system in the near future.

## Acknowledgments

The support of National Natural Science Foundation of China (No. 51975568), National Natural Science Foundation of Jiangsu Province (No. BK20191341), Taishan Scholar (tsqn201812025), Science and Technology Plan of Lianyungang (No. CG1615), Australia ARC DECRA (No. DE190100931) and Priority Academic Program Development of Jiangsu Higher Education Institutions (PAPD) in carrying out this research are gratefully acknowledged.

## Conflict of interests

The authors declare that there is no conflict of interests regarding the publication of this article.

## ORCID iDs

Shuaishuai Sun <https://orcid.org/0000-0002-8695-9217>  
 Zhixiong Li <https://orcid.org/0000-0002-7265-0008>  
 Weihua Li <https://orcid.org/0000-0002-6190-8421>

## References

- [1] Du X M, Yu M, Fu J, Peng Y X, Shi H F and Zhang H 2019  $H_\infty$  control for a semi-active scissors linkage seat suspension with magnetorheological damper *J. Intell. Mater. Syst. Struct.* **30** 708–21
- [2] Bai X X, Cai F L and Chen P 2019 Resistor-capacitor (RC) operator-based hysteresis model for magnetorheological (MR) dampers *Mech. Syst. Signal Process.* **117** 157–69
- [3] Zamani A A, Tavakoli S, Etedali S and Sadeghi J 2019 Modeling of a magneto-rheological damper: an improved multi-state-dependent parameter estimation approach *J. Intell. Mater. Syst. Struct.* **30** 1178–88
- [4] Zhu H, Rui X, Yang F, Zhu W and Wei M 2019 An efficient parameters identification method of normalized Bouc–Wen model for MR damper *J. Sound Vib.* **448** 146–58
- [5] Deng H, Deng J, Yue R, Han G, Zhang J, Ma M and Zhong X 2019 Design and verification of a seat suspension with variable stiffness and damping *Smart Mater. Struct.* **28** 065015
- [6] Bharathi Priya C and Gopalakrishnan N 2019 Temperature dependent modelling of magnetorheological (MR) dampers using support vector regression *Smart Mater. Struct.* **28** 025021
- [7] Duchanoy C A, Moreno-Armendáriz M A, Moreno-Torres J C and Cruz-Villar C A 2019 A deep neural network based model for a kind of magnetorheological dampers *Sensors* **19** 1333
- [8] Nguyen S D and Choi S B 2012 A new neuro-fuzzy training algorithm for identifying dynamic characteristics of smart dampers *Smart Mater. Struct.* **21** 085021
- [9] Nguyen S D, Kim W, Park J and Choi S B 2017 A new fuzzy sliding mode controller for vibration control systems using integrated-structure smart dampers *Smart Mater. Struct.* **26** 045038
- [10] Kumar A and Joshi R 2019 Modelling and analysis of magneto-rheological damper for maximizing the damping force *Advances in Engineering Design* (Singapore: Springer) pp 73–82
- [11] He Y, Liang G, Xue B, Peng Z and Wei Y 2019 A unified MR damper model and its inverse characteristics investigation based on the neuro-fuzzy technique *Int. J. Appl. Electromagn. Mech.* **61** 225–45
- [12] Yu J, Dong X, Zhang Z and Chen P 2019 A novel scissor-type magnetorheological seat suspension system with self-sustainability *J. Intell. Mater. Syst. Struct.* **30** 665–76
- [13] Deng L, Sun S, Christie M D, Yang J, Ning D, Zhu X, Du H, Zhang S and Li W 2019 Experimental testing and modelling of a rotary variable stiffness and damping shock absorber using magnetorheological technology *J. Intell. Mater. Syst. Struct.* **30** 1453–65
- [14] Meng F, Zhou J, Jin C and Ji W 2019 Modeling and experimental verification of a squeeze mode magnetorheological damper using a novel hysteresis model *Proc. Inst. Mech. Eng. C* (<https://doi.org/10.1177/0954406219842906>)
- [15] Han Y, Dong L and Hao C 2019 Experimental analysis and mathematical modelling for novel magnetorheological damper design *Int. J. Appl. Electromagn. Mech.* **59** 367–76

- [16] Wang Y and Fan Y 2010 Adaptive prediction algorithm to improve BP neural network *Comput. Eng. Appl.* **17** 23–6
- [17] Xie Y, Zhang J, He Y, Cheng A and Yin Q 2016 Study on FOA\_BP remote sepsis diagnosis based on wireless sensor network *J. Intell. Fuzzy Syst.* **31** 2737–43
- [18] Mousavi S M, Alikar N and Niaki S T A 2016 An improved fruit fly optimization algorithm to solve the homogeneous fuzzy series–parallel redundancy allocation problem under discount strategies *Soft Comput.* **20** 2281–307
- [19] Liu Q, Zhan M, Chekem F O, Shao X, Ying B and Sutherland J W 2017 A hybrid fruit fly algorithm for solving flexible job-shop scheduling to reduce manufacturing carbon footprint *J. Clean. Prod.* **168** 668–78
- [20] Wang W and Liu X 2015 Melt index prediction by least squares support vector machines with an adaptive mutation fruit fly optimization algorithm *Chemometr. Intell. Lab. Syst.* **141** 79–87
- [21] Pan Q K, Sang H Y, Duan J H and Gao L 2014 An improved fruit fly optimization algorithm for continuous function optimization problems *Knowl.-Based Syst.* **62** 69–83
- [22] Wu L, Liu Q, Tian X, Zhang J and Xiao W 2018 A new improved fruit fly optimization algorithm IAFOA and its application to solve engineering optimization problems *Knowl.-Based Syst.* **144** 153–73
- [23] Yu J, Dong X and Zhang Z 2017 A novel model of magnetorheological damper with hysteresis division *Smart Mater. Struct.* **26** 105042
- [24] Krauze P and Wyrwał J 2014 Magnetorheological damper dedicated modelling of force–velocity hysteresis using all-pass delay filters *Advances in Systems Science*. (Cham: Springer) pp 425–33
- [25] Choi S B, Lee S K and Park Y P 2001 A hysteresis model for the field-dependent damping force of a magnetorheological damper *J. Sound Vib.* **245** 375–83
- [26] Seong M S, Choi S B and Han Y M 2009 Damping force control of a vehicle MR damper using a Preisach hysteretic compensator *Smart Mater. Struct.* **18** 074008
- [27] Dominguez A, Sedaghati R and Stiharu I 2004 Modelling the hysteresis phenomenon of magnetorheological dampers *Smart Mater. Struct.* **13** 1351
- [28] Domínguez-González A, Stiharu I and Sedaghati R 2014 Practical hysteresis model for magnetorheological dampers *J. Intell. Mater. Syst. Struct.* **25** 967–79
- [29] Khalid M, Yusof R, Joshani M, Selamat H and Joshani M 2014 Nonlinear identification of a magneto-rheological damper based on dynamic neural networks *Comput.-Aided Civ. Infrastruct. Eng.* **29** 221–33
- [30] Ni Y Q, Chen Z H and Or S W 2015 Experimental identification of a self-sensing magnetorheological damper using soft computing *J. Eng. Mech.* **141** 04015001
- [31] Nguyen S D and Choi S B 2015 Design of a new adaptive neuro-fuzzy inference system based on a solution for clustering in a data potential field *Fuzzy Sets Syst.* **279** 64–86
- [32] Ayala H V H and dos Santos Coelho L 2016 Cascaded evolutionary algorithm for nonlinear system identification based on correlation functions and radial basis functions neural networks *Mech. Syst. Signal Process.* **68** 378–93
- [33] Imaduddin F, Mazlan S A, Zamzuri H and Fatah A Y A 2016 Testing and parametric modeling of magnetorheological valve with meandering flow path *Nonlinear Dyn.* **85** 287–302
- [34] Hemanth K, Kumar H and Gangadharan K V 2018 Dynamic analysis of half car model with MR damper as semi-active suspension element *Int. J. Acoust. Vib.* **23** 138–46
- [35] Zhao Y L and Xu Z D 2018 A hysteretic model considering Stribeck effect for small-scale magnetorheological damper *Smart Mater. Struct.* **27** 065021
- [36] Niu J, Zhong W, Liang Y, Luo N and Qian F 2015 Fruit fly optimization algorithm based on differential evolution and its application on gasification process operation optimization *Knowl.-Based Syst.* **88** 253–63
- [37] Liu X, Shi Y and Xu J 2017 Parameters tuning approach for proportion integration differentiation controller of magnetorheological fluids brake based on improved fruit fly optimization algorithm *Symmetry* **9** 109
- [38] Xu J, Wang Z, Tan C, Si L, Zhang L and Liu X 2016 Adaptive wavelet threshold denoising method for machinery sound based on improved fruit fly optimization algorithm *Appl. Sci.* **6** 199
- [39] Han X, Liu Q, Wang H and Wang L 2018 Novel fruit fly optimization algorithm with trend search and co-evolution *Knowl.-Based Syst.* **141** 1–17
- [40] Lei X, Ding Y, Fujita H and Zhang A 2016 Identification of dynamic protein complexes based on fruit fly optimization algorithm *Knowl.-Based Syst.* **105** 270–7
- [41] Zheng X L and Wang L 2016 A knowledge-guided fruit fly optimization algorithm for dual resource constrained flexible job-shop scheduling problem *Int. J. Prod. Res.* **54** 5554–66
- [42] Zhang R, Duan Y, Zhao Y and He X 2018 Temperature compensation of elasto-magneto-electric (EME) sensors in cable force monitoring using BP neural network *Sensors* **18** 2176
- [43] He F and Zhang L 2018 Prediction model of end-point phosphorus content in BOF steelmaking process based on PCA and BP neural network *J. Process Control* **66** 51–8
- [44] Ding S, Su C and Yu J 2011 An optimizing BP neural network algorithm based on genetic algorithm *Artif. Intell. Rev.* **36** 153–62